Tailoring of the Nanotexture of Mesoporous Silica Films and Their Functionalized Derivatives for Selectively Harvesting Low Molecular Weight Protein

Ye Hu,[†,∥] Ali Bouamrani,[†,∥] Ennio Tasciotti,[†] Li Li,[‡] Xuewu Liu,[†,*] and Mauro Ferrari[†,§,⊥,*]

[†]Department of Nanomedicine and BioMedical Engineering, The University of Texas Health Science Center at Houston, Houston, Texas 77030, [‡]Research Center of Protein Chemistry and Proteomic Core Laboratory, Brown Institute of Molecular Medicine, The University of Texas Health Science Center at Houston, Houston, Texas 77030, [§]Department of Experimental Therapeutics, The University of Texas MD Anderson Cancer Center, Houston, Texas 77030, and [⊥]Department of Bioengineering, Rice University, Houston, Texas 77030. [∥]Shared first authorship.

ABSTRACT We present a fast, efficient, and reliable system based on mesoporous silica chips to specifically fractionate and enrich the low molecular weight proteome. Mesoporous silica thin films with tunable features at the nanoscale were fabricated using the triblock copolymer template pathway. Using different templates and concentrations in the precursor solution, various pore size distributions, pore structures, and connectivity were obtained and applied for selective recovery of low mass proteins. In combination with mass spectrometry and statistic analysis, we demonstrated the correlation between the nanophase characteristics of the mesoporous silica thin films and the specificity and efficacy of low mass proteome harvesting. In addition, to overcome the limitations of the prefunctionalization method in polymer selection, plasma ashing was used for the first time for the treatment of the mesoporous silica surface prior to chemical modification. Surface charge modifications by different functional groups resulted in a selective capture of the low molecular weight proteins from serum sample. In conclusion, our study demonstrates that the ability to tune the physicochemical properties of mesoporous silica surfaces, for a selective enrichment of the low molecular weight proteome from complex biological fluids, has the potential to promote proteomic biomarker discovery.

KEYWORDS: mesoporous silica thin film · low molecular weight proteome · nanotexture · chemical modification · mass spectrometry · early diagnostics

Mesoporous silica (MPS) thin film made by self-assembly of the triblock copolymer (poly(ethylene oxide) (PEO)−poly(propylene oxide) (PPO)−poly(ethylene oxide) (PEO)) with hydrolyzed silicate precursors has generated substantial interests.[1−4] Different mesoporous materials were investigated in applications such as high surface area catalysis,[5−8] molecular sieves,[9−12] gas sensors,[13] optoelectronic devices,[14−17] and drug delivery.[18−22] Due to its well-defined pore network and surface reactivity, mesoporous silica was extensively studied for the absorption and separation of biological molecules.[23−25] The principal methodology for the synthesis of mesoporous silica is focused on evaporation-induced self-assembly (EISA).[26] Starting with homogeneous, hydro-alcoholic solutions of soluble silicate (TEOS, tetraethoxysilane) and a structure-directing polymer, the preferential evaporation of the solvent after dip or spin coating drives silica/copolymer self-assembly into a uniform thin film nanophase by increasing the concentration of polymer to exceed the critical micelle concentration. After removing the organic template by calcination, mesoporous films with narrow nanoscale pore size distribution and high ratio of surface area to pore volume are formed.

We have previously demonstrated the use of mesoporous silica surfaces as a size exclusion method for harvesting the peptides and small proteins.[27−30] The identification of circulating biomarkers holds great potential for noninvasive approaches in early detection and prognosis, as well as for the monitoring of therapeutic efficiency.[31−35] The circulating low molecular weight proteome (LMWP), composed of small proteins shed from tissues and cells or peptide fragments derived from the proteolytic degradation of larger proteins, has been associated with the pathological condition in patients.[36−38] Despite these potential clinical applications, the use of matrix-assisted laser desorption/ionization time-of-flight mass spectrometry (MALDI TOF MS) to profile the LMWP from

*Address correspondence
mauro.ferrari@uth.tmc.edu,
xuewu.liu@uth.tmc.edu.

Received for review September 29, 2009 and accepted December 10, 2009.

Published online December 16, 2009.
10.1021/nn901322d

biological fluids remains a major technical challenge due to the large dynamic range of protein and peptide concentrations in serum.[39] Without sample pretreatment, the highly abundant proteins impede the detection of low-abundance species in serum/plasma. Current proteomic-based approaches, such as two-dimensional polyacrylamide gel electrophoresis (2D-PAGE) and shotgun proteomics methods, are labor-intensive and low throughput, offering limited suitability for clinical applications.[40−42] Therefore, more effective strategies are needed to isolate circulating LMWP and allow the high throughput screening of clinical samples.

In the present study, to improve both selectivity and sensitivity of peptide recovery for the specific target in clinical use, we designed and characterized a large set of MPS thin films with various pore nanotextures and surface modifications to enhance the capacity and efficiency of low-abundance LMWP enrichment. One of the promising characteristics of MPS thin films is the variety of achievable pore configuration, which mainly depends on the molecular weight of the block copolymer, the ratio of the hydrophilic (PEO) to hydrophobic (PPO) block volume in the amphiphilic polymer, and the proportion of the polymer in the starting material.[3] We selected four typical triblock copolymers with different molecular weights and compositions: $PEO_5-PPO_{70}-PEO_5$ (Pluronic L121), $PEO_{20}-PPO_{70}-PEO_{20}$ (Pluronic P123), $PEO_{106}-PPO_{70}-PEO_{106}$ (Pluronic F127), $PEO_{13}-PPO_{30}-PEO_{13}$ (Pluronic L64). These were used as the synthetic templates to form the MPS thin films with diversified pore size and structural properties. Furthermore, the addition of a hydrophobic polymer to the precursor solution modifies the ratio of hydrophobic/hydrophilic blocks and thus enlarges the MPS pore size. In this study, poly(propylene glycol) (PPG) was used as a swelling agent to extend pore size up to 7 nm and increase porosity to 67% for the thin film prepared with L121. By tuning the amount of Pluronic F127 copolymer in solution, the periodic nanostructure can be transformed from a three-dimensional (3D) cubic or a 3D hexagonal to a two-dimensional (2D) hexagonal framework. Furthermore, to achieve selective electrostatic harvesting of LMW proteins, we conjugated several organic trialkoxysilanes on the MPS surface. The conventional approaches to synthesize hybrid organic−inorganic nanocomposites, including one-pot synthesis[43−47] and postgrafting method,[5,48−50] are not suitable for our MPS application because of either their low loading content (postgrafting) or the limited selection of polymer templates (one-spot). Herein, we improved the method of conjugating various organosilane compounds on the mesoporous silica chips. On the basis of the postgrafting approach, plasma ashing was used for the first time for the treatment of the mesoporous silica surface prior to chemical modification. The results show the improvement of functional group loading and the compatibility of this method for all synthetic templates and organosilanes.

The study presented in this paper reveals the potential of the MPS-based technology to provide a powerful alternative to conventional methods for LMWP enrichment from complex biological fluids. Because of the ability to tune the material properties, the capability for low-cost production, the simplicity and rapidity of sample processing, and the greatly reduced sample requirements for analysis, this novel nanotechnology will substantially impact the field of proteomic biomarker research and clinical proteomic assessment.

RESULTS AND DISCUSSION

Fabrication and Characterization of Mesoporous Silica Thin Films. Most of the procedures used for the synthesis of mesoporous silica films are similar to the ones described by Zhao *et al.*[2] The primary objective of this study was to tailor MPS thin film pore morphology and internal structure by adjusting synthetic parameters and to explore their efficacy for the specific harvesting of LMWP species from human serum. A consistent proteomic profiling approach requires that the MPS-based serum fractionation be performed with a well-defined, high purity substrate possessing good thermal stability as well as uniform nanostructure and film thickness throughout the entire mesoporous silica layer. The preparation of the precursor solution, involving the cooperative assembly of a polymer surfactant and soluble silicate species, plays a dominant role in determining the molecular organization of the final product (see Supporting Information Table 1 for molar ratios of starting materials for each block copolymer used). To prevent shrinkage of the MPS, the deposited film thickness did not exceed 1 μm. This was accomplished by maintaining the molar ratio of ethanol to silicate between 12 and 14 and water to silicate at less than 6. The pH of the precursor solution was kept in the range of 1.2 to 1.5 in order to avoid the precipitation of silicate and to achieve equilibrium between the condensation of silicate onto the polymer micelles and its hydrolysis in solution. Porosity and pore structure were adjusted by changing the molar ratio of the polymers in the mixture. Spin coating, superior to other deposition techniques for achieving uniform thickness and porosity, was used to form the MPS thin films on a silicon substrate. Because of the weak interaction between molecules during the self-assembly process, substantial non-uniformity of mesoporous silca products can result from inadequately controlled synthesis.[3] Experimental parameters, such as aging time of the precursor solution, coating speed during solution deposition, and calcination temperature can impact the final features of the mesoporous structure. To investigate the effect on pore geometry and connectivity, we adjusted the amphiphilic structure of the block copolymers and

their concentration in the precursor solution, with all other process parameters kept constant.

We characterized pore architectures and physicochemical properties of MPS thin films with ellipsometry, one-dimentional X-ray diffraction (1D-XRD), N_2 adsorption/desorption, transmission electron microscopy (TEM), X-ray photoelectron spectroscopy (XPS), and surface contact angle goniometry. The overall purity and the atomic silicon-to-oxygen ratio of the MPS thin films prepared with L121 are illustrated with the Si 2p, O 1s, and C 1s regions of the XPS spectra (Figure 1). The weak signal for the C 1s region demonstrates the minimal hydrocarbon contamination on the film surface. Both the Si 2p and O 1s regions present a sharp and symmetric single peak at binding energies around 101.4 and 530.7 eV, respectively, which strongly points to a silica framework with high condensation. By calculating the areas under the peaks for Si 2p and O 1s, an atomic silicon-to-oxygen ratio of 1:2.004 was obtained, further confirming the high purity of MPS thin films. The nearly but not perfectly symmetric shape of the O 1s peak is because the observed peak is a actually a combination of two sets of peaks—the dominant one came from Si−O and the subordinated one was obtained from the Si−OH group on the silica wall (see Figure S.1). Similar XPS results were acquired for MPS thin films synthesized using the different polymer templates.

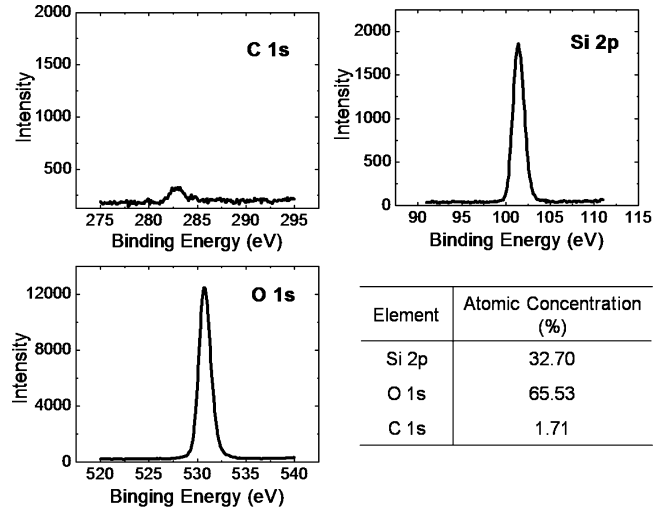

Element	Atomic Concentration (%)
Si 2p	32.70
O 1s	65.53
C 1s	1.71

Figure 1. Purity of MPS thin films. XPS core level spectra used to analyze the relative amounts of C, Si, and O on the surface of a mesoporous silica thin film prepared with Pluronic L121. The tabulated atomic concentration of each element is shown in the lower right.

Serum Fractionation on Mesoporous Silica Thin Films. The protocol for serum fractionation using the MPS thin films is described in the Methods. Briefly, the serum sample is spotted on the MPS chip and incubated at room temperature for 30 min. LMW molecules are trapped in the pores, while the larger proteins are removed from the surface after multiple washings with deionized water. The captured molecules are eluted from the pores using an acidic solution and analyzed by MALDI TOF MS (see Supporting Information Figure S.2). Since all peptides and proteins become positively charged after being eluted with 1% TFA, we use the positive mode in MOLDI for a more sensitive detection of protein signals. Figure 2a,b shows the MS spectra of the unprocessed serum sample for peptides in the range of 900 to 10 000 Da and for proteins in the range of 3000 to 70 000 Da, respectively. These spectra illustrate the signal suppression in the LMW region due to the presence of highly abundant, high molecular weight (HMW) proteins such as albumin. Figure 2c,d depicts the MS spectra of the serum sample after fractionation by the MPS thin films synthesized using L121 and swelling agent PPG at a molar ratio of 1:0.5. Depletion of the large molecules and the enrichment of the LMW components resulted in a significant improvement of MS detection in the low mass range. As a control, the same serum sample was applied onto a nonporous pure silica surface to evaluate the advantage of MPS thin films for LMWP recovery. As can be seen in Figure 2e,f, there was no significant harvesting of peptides or proteins with the nonporous silica. Thus, it can be concluded that it was the mesoporous architecture and not the silica surface affinity that constitutes the predominate factor in the enrichment of LMWP.

Reproducibility of Serum Fractionation on Mesoporous Silica Thin Films. Concerns have been raised about analytical bias generated by sample handling and sample pretreatmnent procedures in the proteomic profiling studies.[51−53] Therefore, fractionation reproducibility and reliability are mandatory for any further development of reliable proteomic and peptidomic screening techniques for clinical applications.[54,55] To assess the consistency of our on-chip fractionation strategy, we screened six replicates with six aliquots of the same human serum sample using MPS thin films prepared by L121+PPG with a molar ratio of 1:0.5. The MS profiles for recovered species in the ranges of peptide and proteins are, respectively, displayed in Figure S.3a,b in the Supporting Information. The general variability of the peak signals is illustrated on the histogram displaying the repartition of the coefficients of variation (CV) measured for each detected peak (Figure 3a). The average CV was estimated at 13.1%, which demonstrated a high reproducibility for the detected peaks over a wide mass range of 800 to 20 000 Da. The regression curve and equation comparing the peak intensities recovered from the replicates are illustrated in Figure 3b and exhibit a coefficient of regression $R^2 = 0.988$. These results confirmed that the on-chip serum fractionation did not induce any significant variability in the sample and demonstrated the reliability of our MPS chips in the pretreatment of complex biological samples.

Effect of Pore Structure and Distributional Architecture on LMWP Recovery. One main advantage of block copolymers with high molecular weight is their ability to form a variety of structures by tuning experimental condi-

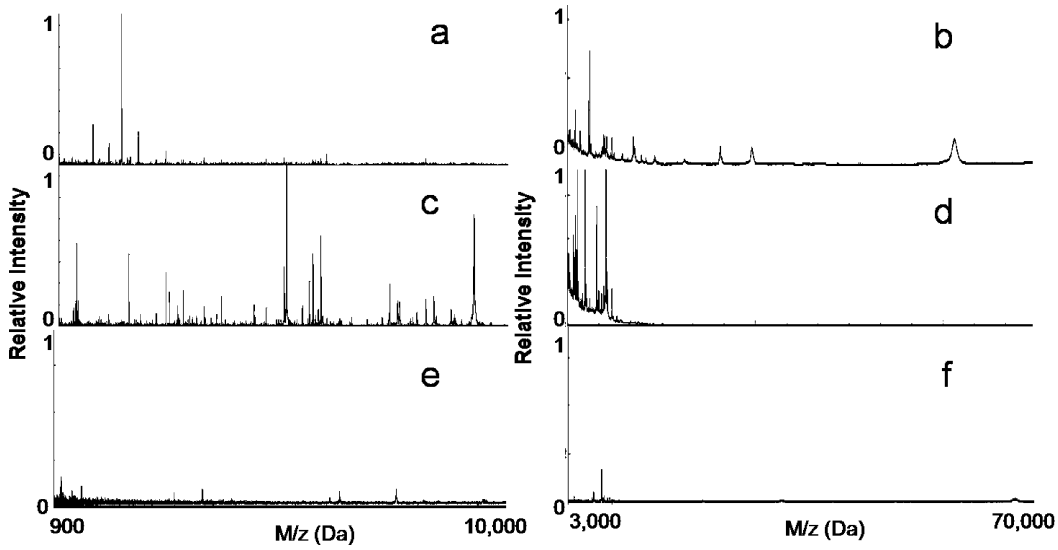

Figure 2. Peptide enrichment using the mesoporous silica thin film chips. MALDI MS profiles in both the low mass range (900 to 10 000 Da) and the high mass range (3000 to 70 000 Da) before (a,b) and after (c,d) serum processing on the mesoporous silica thin films. The molecular recovery is significantly reduced when using blank nonporous silica surfaces (e,f).

tions during MPS thin film synthesis. The structural transformation of the mesoporous arrangement was carried out by tuning the concentration of the template polymer. Increasing the concentration of the template polymer resulted in a reduced interfacial curvature between the phases of the water, the copolymer, and the silicate, consequently initiating the inter-related progression from a spherical to a cylindrical structure. Pluronic F127, with its high molecular weight, possesses this high degree of structural periodicity. In this study, the concentrations of all starting materials, except F127, were kept constant. Figure 4 demonstrates the changes in the nanostructure of the MPS by characterization through XRD pattern, TEM imaging, and N_2 adsorption/desorption analysis. When the F127 concentration in the precursor solution was kept at 4.0×10^{-3} M, the final MPS thin film acquired a 3D cubic structure with reflection peaks at (100) and (110) and a low intensity peak at (220) as indicated by the XRD pattern (Figure 4a) and further verified through TEM imaging (inset of Figure 4a). N_2 adsorption/desorption curves were generated using a Quantachrome Autosorb-3b BET surface analyzer (inset of Figure 4b), and the pore size distribution was calculated using the Barrett−Joyner−Halenda (BJH) method[56] (Figure 4b). The adsorption/desorption isotherms describe a type IV isotherm with a H2 hysteresis loop (sloping adsorption branch and nearly vertical desorption branch), indicating a nanoporous structure with interconnecting channels. Inflection points appearing at $0.40 \leq P/P_0 \leq 0.75$ in the figure indicated the formation of ink-bottle shape nanopores. Increasing the F127 concentration to 6.0×10^{-3} M yields a 3D honeycomb-like nanostructure hexagonally arranged on the substrate, as confirmed by XRD, with peaks at (200) and (400) (Figure 4c), and TEM imaging (Figure 4c inset). The adsorption/desorption isotherms, depicted with the pore size distribution in the inset of Figure 4d, vary slightly from the similar adsorption−desorption type VI isotherms described for the lower concentration F127 MPS thin films due to the increased internal pore connectivity. A further increase of the F127 concentration to 8.0×10^{-3} M resulted in a 2D hexagonal nanostructure parallel to the substrate surface as confirmed by the sharp peaks at (100) and (300) in the XRD

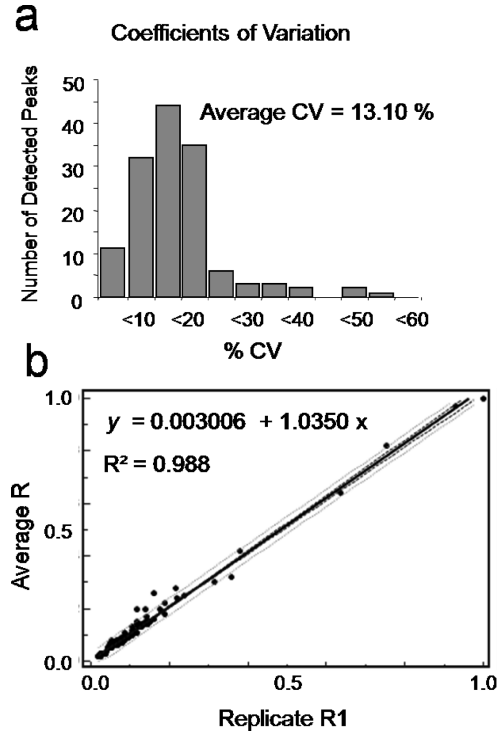

Figure 3. Reproducibility of on-chip enrichment. (a) Coefficient of variation (CV) distribution of MS intensities for detected peaks. The average CV is indicated. (b) Linear regression analysis of average intensities of detected MS peak in each replicate compared to replicate 1. The equation and the coefficient of determination (R^2) are presented.

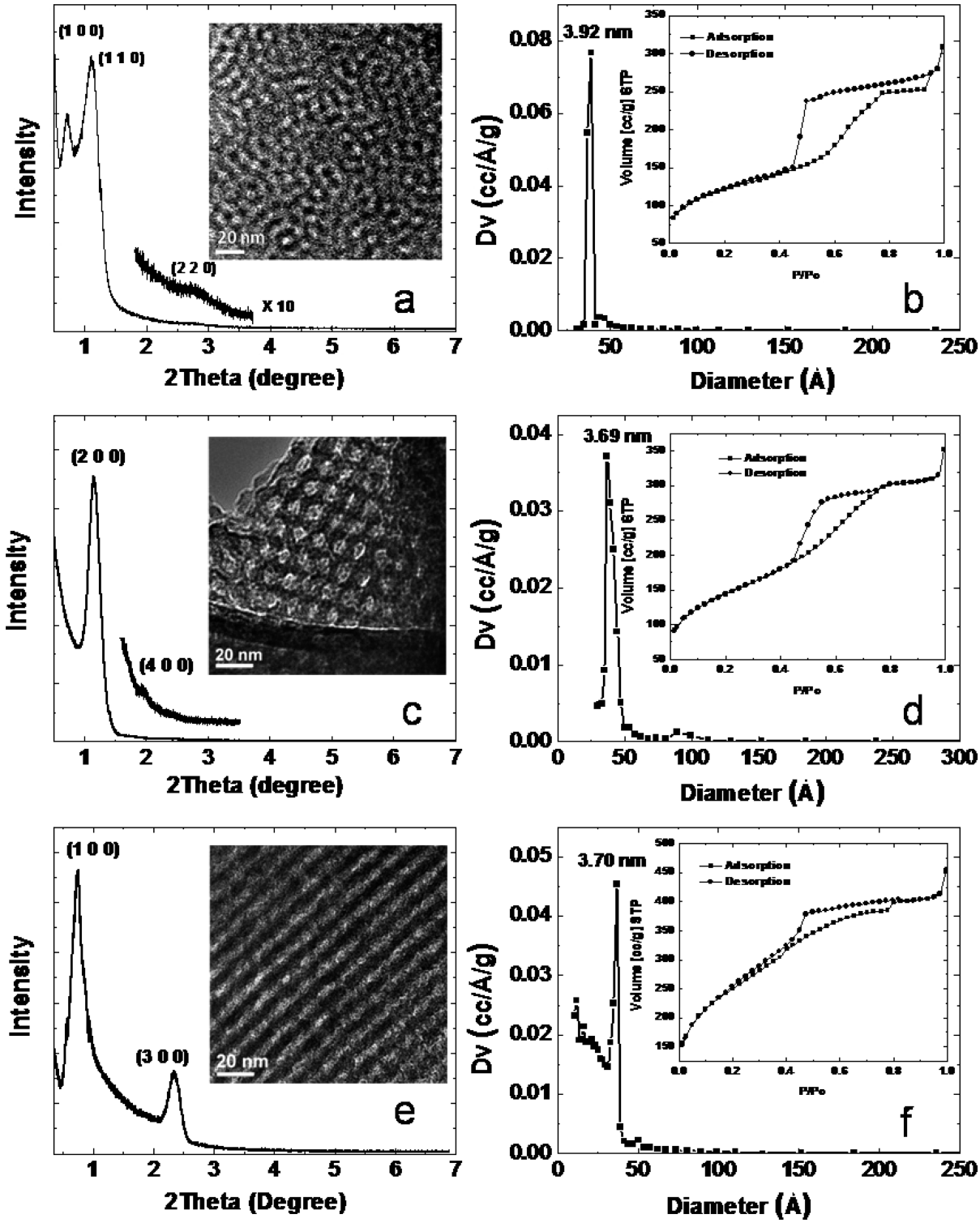

Figure 4. Physical characterizations of MPS thin films. XRD patterns (a,c,e), TEM (inset a,c,e), and N_2 adsorption/desorption analysis (pore size distribution in b,d,f, isotherms in the insets of b,d,f) of the structural transformation of mesoporous thin films prepared using Pluronic F127 at different concentrations in the precursor solution: 4.0×10^{-3} M (a,b), 6.0×10^{-3} M (c,d), and 8.0×10^{-2} M (e,f).

pattern (Figure 4e) and TEM imaging (Figure 4e inset). The adsorption/desorption isotherms (Figure 4f inset) display a narrow hysteresis loop, indicating lower interpore connectivity. The similar pore size distributions of the three different nanostructures, with average pore sizes around 3.7 nm, illustrate that the change of pore size was minimally dependent on the molar ratios of the starting materials.

We investigated the effect of the structural variation of the mesoporous F127 nanochips (3D cubic, honeycomb hexagonal, and 2D hexagonal) on the enrichment of LMW species. The three different

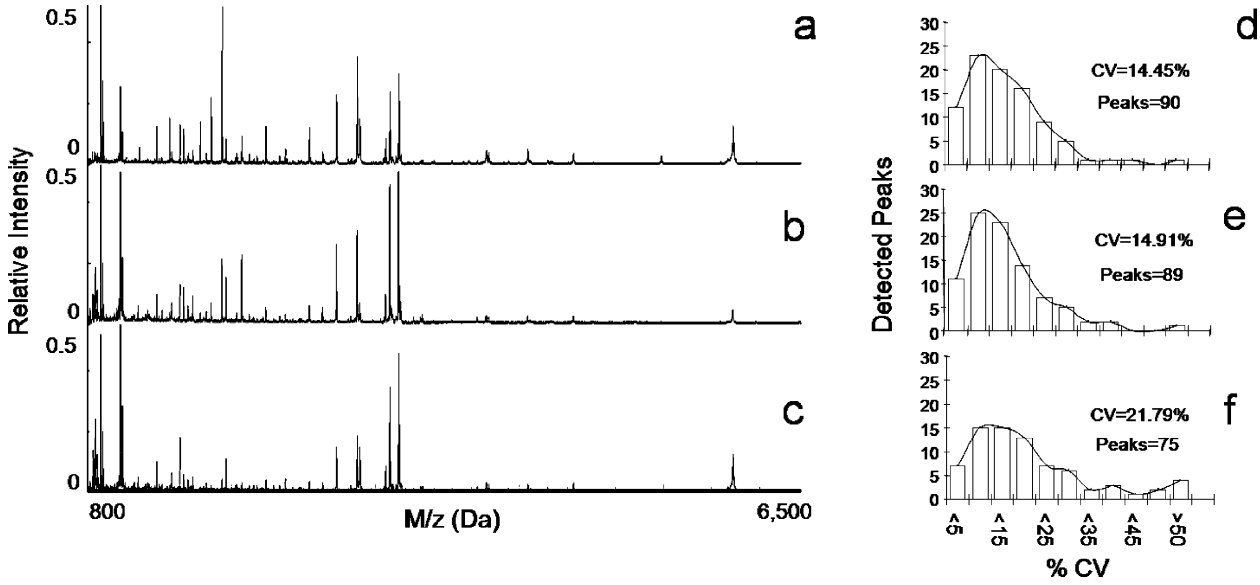

Figure 5. Effect of pore structural transformation on LMWP recovery from F127 chips. The MALDI profiles for the (a) 3D cubic, (b) 3D honeycomb hexagonal, and (c) 2D hexagonal nanoscale morphologies. The coefficient of variation (CV) distributions of MS peak intensities for each of the MALDI profiles is also shown (d−f). The average CV and the number of detected peaks are indicated in each histogram.

nanostructures possess similar pore size distributions (3.7 to 3.9 nm) and exhibit the same molecular cutoff, demonstrating the same size exclusion property (see Supporting Information Figure S.4). For both 3D nanoporous morphologies, the increased pore connectivity and the reduced steric hindrance imposed on the diffusion of peptides and proteins resulted in higher recovery efficacy. The dramatic difference between 3D nanostructures and 2D hexagonal framework in the MS profiles for peptides recovery in the range of 800−10 000 Da is shown in Figure 5a−c. The average CV for 3D cubic structure (Figure 5d) or 3D honeycomb hexagonal structure (Figure 5e) is significantly lower than the average CV of the 2D hexagonal architecture (Figure 5f), which shows a broader CV distribution. These results indicate that the serum fractionation on the MPS thin film with a 3D nanotexture possesses a comparatively lower variability because of the greater pore connectivity of 3D structures. In addition, to demonstrate the differential harvesting capacity of the different pore architecture, we fractionated a solution of known molecular standards (see Supporting Information Table 2) on the 3D cubic and 3D hexagonal MPS. As shown in Figure 6, there is selective peptide enrichment as illustrated by the significant increase of the capture of ACTH and insulin peptides on the hexagonal surface while substance P and α-endorphin peptides are specifically recovered from the cubic MPS.

Effect of Selecting Polymer Template on LMWP Recovery. Another factor that influences the interfacial curvature between the polymer and the other solution components (TEOS, water, *etc.*), and thus determines the nanostructure and the pore size, is the hydrophilic/hydrophobic volume ratio of the copolymer. Triblock copolymers with different hydrophobic (PPO) to hydrophilic (PEO) volume ratios were selected to synthesize MPS thin films with different pore sizes and nanostructures and subsequently investigated for their LMWP harvesting efficacy. Block copolymer compositions with longer PPO block lengths lead to increased pore size. Longer PEO block lengths for a given PPO block length (L121 *versus* P123 *versus* F127) lead to the formation of more ordered periodic nanostructures.[3] L-type (liquid phase) block copolymers (such as L64 and L121) with

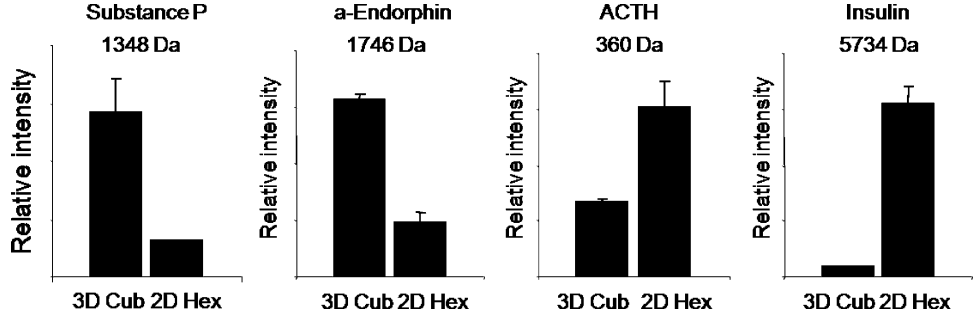

Figure 6. Selective recovery with different nanostructures. Bar graph of the intensity of detection illustrating the selective peptides recovery on 3D cubic and 3D hexagonal F127 proteomic chips (Cub and Hex, respectively). The different structural modifications present a selective enrichment.

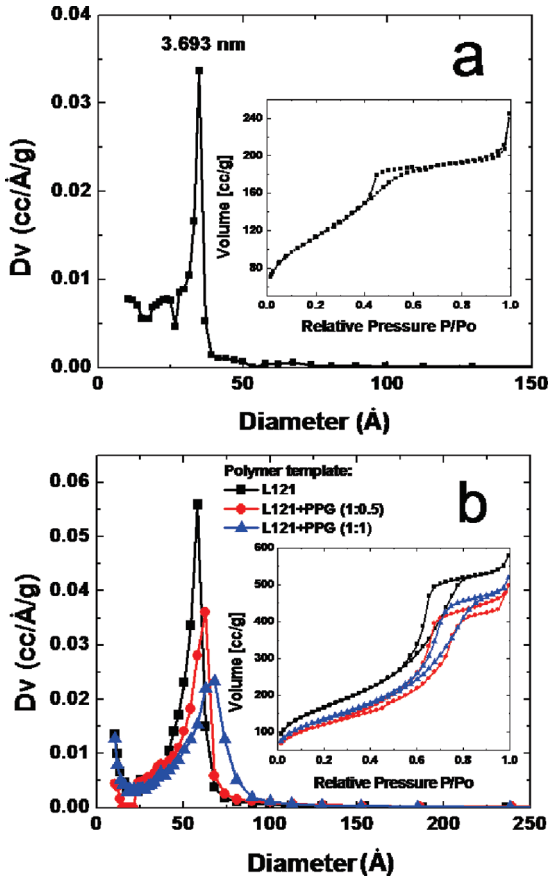

Figure 7. Pore size tuned with polymer templates. Pore size distribution of mesoporous silica thin films prepared with different triblock copolymer templates and the corresponding adsorption/desorption isotherm (inset): (a) P123; (b) L121 and L121 with swelling agent (PPG) at molar ratios of 0.5 and 1.0.

lower PEO block lengths offer increased porosity due to their greater deforming performance but more chaotic nanostructure. Figure S.5 in the Supporting Information displays XRD patterns with the scanning transmission electron microscopy (STEM) imaging (insets) performed for MPS thin films prepared from P123, F127, L64, and L121+PPG (with molar ratio of 1:0.5) detailing their internal nanoscale organization. N_2 adsorption−desorption isotherms were measured to assess pore size distribution and total surface area of the MPS thin films. The BJH pore size distributions for chips prepared by P123 (Figure 7a) and L121 (Figure 7b) are provided, each depicting low pore size dispersion as denoted by their sharp distribution peaks, along with their adsorption/desorption isotherms (insets). Figure 7a shows type IV adsorption/desorption isotherms with well-defined H2 hysteresis loops. The MPS thin films prepared using P123 and F127 possess similar mean pore size (~3.7 nm) due to their identical PPO block volume, but the MPS prepared with P123 possesses a poor connectivity indicated by its narrow hysteresis loop. Shown in Figure 7b for chips prepared with L121, the pore diameter distribution peaks shift from 5.82 to 6.79 nm with increasing amounts of the swelling agent. Their adsorption/desorption isotherms were also type IV but with a H1 hysteresis loop attributed to cylindrically shaped pores. Addition of PPG did not result in any change in the loop shape, indicating that the inner pore connectivity is not altered by the swelling agent. Although the MPS thin films prepared with L64 possess similar adsorption/desorption isotherms with L121, its shorter hydrophobic chain (PPO) led to nanopores with smaller pore size (~3.2 nm). The contact angles of MPS thin film surfaces were tested by captive bubble contact angle goniometry to characterize the hydrophilicity of the chips (Supporting Information Figure S.6).

The relatively higher hydrophobicity, smaller pore volume, and poor pore connectivity of the P123 chip presented limited harvesting capability compared to F127 chip with similar pore size (see Supporting Information Figure S.7). With the largest average pore size and the highest surface hydrophilicity, the mesoporous silica chip produced using L121+PPG captured peptides and proteins in a wider molecular mass range. The chips with small pore size prepared with F127 and L64 preferentially enriched the peptides in the lower mass range. To assess this size-dependent ability of the mesoporous silica chips to capture LMWP, a hierarchical clustering analysis of peptides extracted from four different mesoporous silica chips with various pore sizes was performed (Figure 8). The clustering algorithm clearly separates the samples into two major clusters representing specific proteomic patterns for smallest pore and largest pore chips. The high intensity of smaller LMWP was obtained with the chips prepared with L64 and F127 due to their preferred pore sizes, 3.20 and 3.71 nm, respectively. However, the periodic pore structure and uniform small pore size provided by F127 chips demonstrate a more homogeneous enrichment pattern. The mesoporous silica chips prepared by L121 with the pore sizes enlarged using the swelling agent (molar ratios of 50 to 100% PPG to template polymer) offer an increased selective capture of peptides and proteins with higher molecular weight. The larger pore size presented by the L121 with 100% PPG resulted in a more efficient recovery as illustrated by the higher intensity of the enrichment pattern observed on the hierarchical clustering.

Improvement of Chemical Modification on MPS Thin Film and Their Effect on Specific LMWP Recovery. Another approach to improve the enrichment capacity of the MPS chips is to resolve the complexity of biological samples by separating peptides of interest according to their chemical properties. We have developed MPS chips conjugated with chemical functional groups to provide cationic and anionic surfaces. Postgrafting is a straightforward method to add organic groups onto the surface of the pores. MPS possesses many silanol (Si−OH) groups on the surface that can act as convenient anchoring points for organic functionalization. However, high temperature during calcination process may cause a portion of

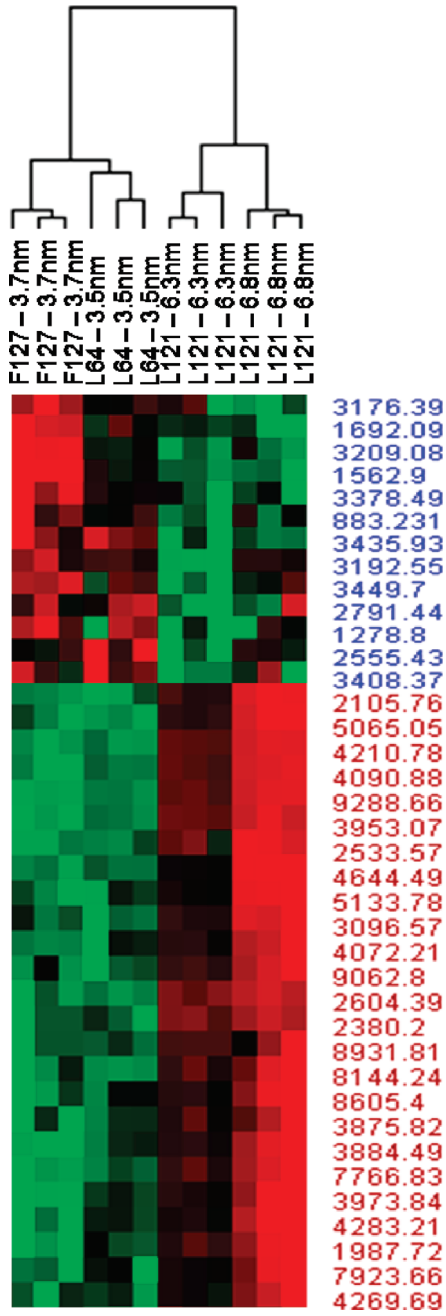

Figure 8. Effect of pore size on LMWP recovery. The supervised hierarchical clustering analysis of peak intensities for samples fractionated using chips prepared with F127, L64, L121 + 50% PPG, and L121 + 100% PPG. Red indicates peak intensities higher than the median value, green is for peak intensities lower than the median value, and black represents peak intensities equal to the median value. Each row represents an individual mass peak (MALDI MS peak), and each column represents a mesoporous thin film chip produced using a specific triblock copolymer.

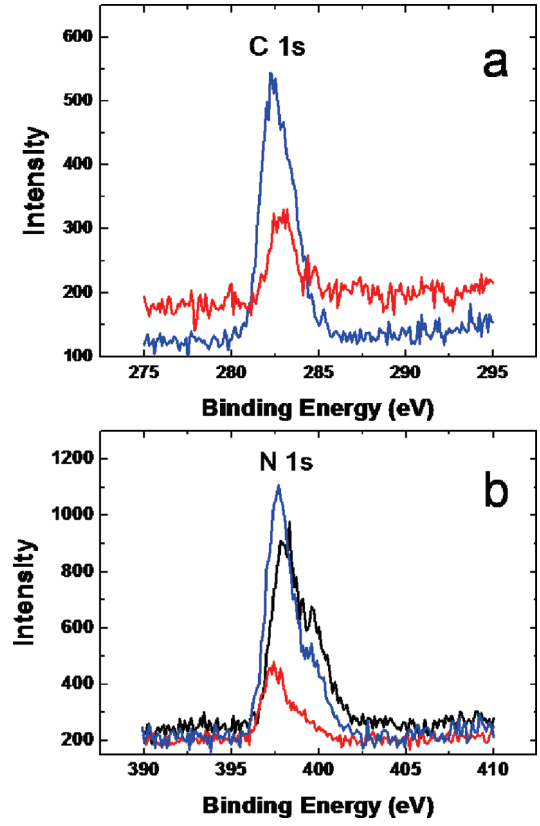

Figure 9. XPS spectra of mesoporous silica chips with APTES modification. (a) Comparison of C content in XPS on the mesoporous silica chips before and after APTES modification. (b) Comparison of N content in XPS on the mesoporous silica chips modified with one-spot synthesis (black curve), modified with postgrafting without pretreatment (red curve) and modified with postgrafting with oxygen plasma treatment (blue curve).

surface silanol groups to be extensively dehydrated, resulting in a substrate incompatible with conjugating organosilane groups. Therefore, more research groups focus their attention on one-spot synthesis. This technology involves co-condensation of tetraalkoxysilanes and organotrialkoxysilanes in the presence of surfactants during synthesis, resulting in higher organic content and a more homogeneous organic distribution in the material. However, co-condensation in one-spot synthesis also caused several difficulties in addition to the control of the main parameters related to the EISA process. For instance, homogeneous solubility of the organic functionalities with silicate precursor in the medium limits the selection of surface modification. On the other hand, one-spot synthesis has a limited interest in our study due to the restricted selection of polymer templates, which must own a different melting point than organotrialkoxysilanes. The participation of organosilane into nanostructured films may also lead to significant damage in the silica network.

To break through the aforementioned limitations, we used oxygen plasma ashing to treat the surface of the mesoporous silica chip before the postgrafting. Plasma ashing is a well-known technique for removing the photoresist in semiconductor manufacturing. Herein the oxygen plasma restored the defective points (Si−H or Si−$(CH_3)_x$) on the MPS surface, generated high-density Si−OH groups, and improved the hydrophilicity (Supporting Information Figures S.8 and S.9). A comparison of XPS intensity in Figure 9a is presented for C content on the APTES-modified chips before and

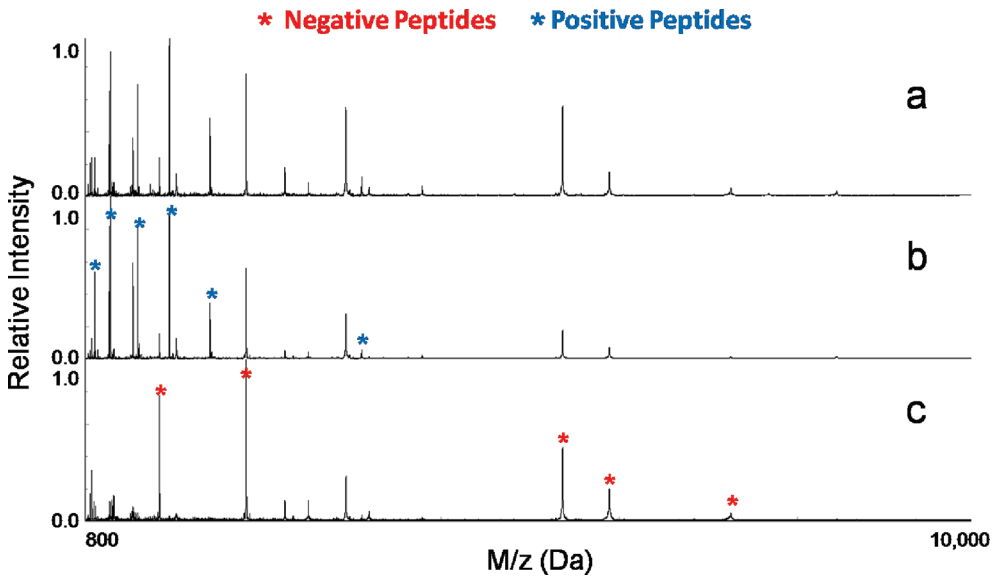

Figure 10. Effects of chips functionalization on the LMW enrichment. MALDI MS profiles of selectively captured peptides on the chemically modified chips. Positively and negatively charged mesoporous thin films specifically enrich negative and positive peptides, respectively.

after chemical modification. The significant increase of C 1s peak for the chips after modification, resulting from the alkyl chain on APTES, validates the efficacy of postgrafting on the chip surface treated with oxygen plasma. Figure 9b exhibits the comparison for N 1s peak on the three mesoporous silica chips APTES-modified under different method (black curve, N 1s on the chips after one-spot modification; red curve, N 1s on the chips after postgrafting without any pretreatment; blue curve, N 1s on the chips after postgrafting method with pretreatment by oxygen plasma). The difference for N 1s peak around the binding energy of 397 eV clearly implies the efficacy of oxygen plasma in grafting the functional groups on the pore surface. The chip that received an oxygen plasma pretreatment is capable of conjugating four times the amino content than a chip without any surface treatment. Although the intensities for N 1s peaks are similar, the chip carried by postgrafting with oxygen plasma pretreatment consisted of a sharper and more symmetric single peak at binding energies around 397 eV, which strongly points to a loading of APTES with high condensation on the pore surface. By the same approach, the functional groups with negative charge, such as thiol, carboxyl, and epoxy, can be conjugated on all the chips in our study with abundant loading (Supporting Information Figures S.10 and S.11). The thickness and porosities for all MPS chips with chemical modification changed slightly due to the conjugation of a thin layer of functional groups, while their nanostructure remained the same as reflected by XRD and TEM.

In order to qualitatively study the electrostatic effect on selective on-chip enrichment, we mixed 26 standard peptides and proteins with a wide range of molecular weights and isoelectric points. MS analysis of the proteomic standard solutions fractionated on MPS chips prepared with L121 and conjugated with the chemical functional groups is presented in Figure 10. The positively charged and negatively charged peptides and LMW proteins are captured on the anionic and the cationic chips, respectively. HMW proteins remain excluded from the chips independently from their charge. For example, albumin has a net negative charge and remains excluded from the cationic chip (Supporting Information Figure S.12). The quantitative comparison of multiple MPS chips in recovering the peptides with positive net charge is displayed in Figure 11a. The chips with negative charge and the chips without any modification (with a minor negative charge originally) exhibit significantly higher enrichment for those peptides than the chips modified with APTES ($-NH_2$). Conversely, the positively charged MPS chips possess exceptional capability to recover those peptides with negative net charge, as demonstrated in Figure 11b, while α-endorphin does not show a significant change due to its PI around 6. These results and the identical molecular cutoff offer displayed by the chips demonstrate the dual properties of the functionalized MSC: (1) the size dependent depletion of HMW proteins by the porous surface; (2) the specific enrichment of differentially charged LMW peptides.

CONCLUSIONS

Evidence is mounting that the low molecular weight region of the circulatory proteome is a rich source of diagnostic biomarkers for the early detection of disease. In this study, we fabricated a series of mesoporous silica thin films with a variety of nanotextures and comprehensively explored their use in selective capturing and enriching the peptides and LMW proteins from human serum.

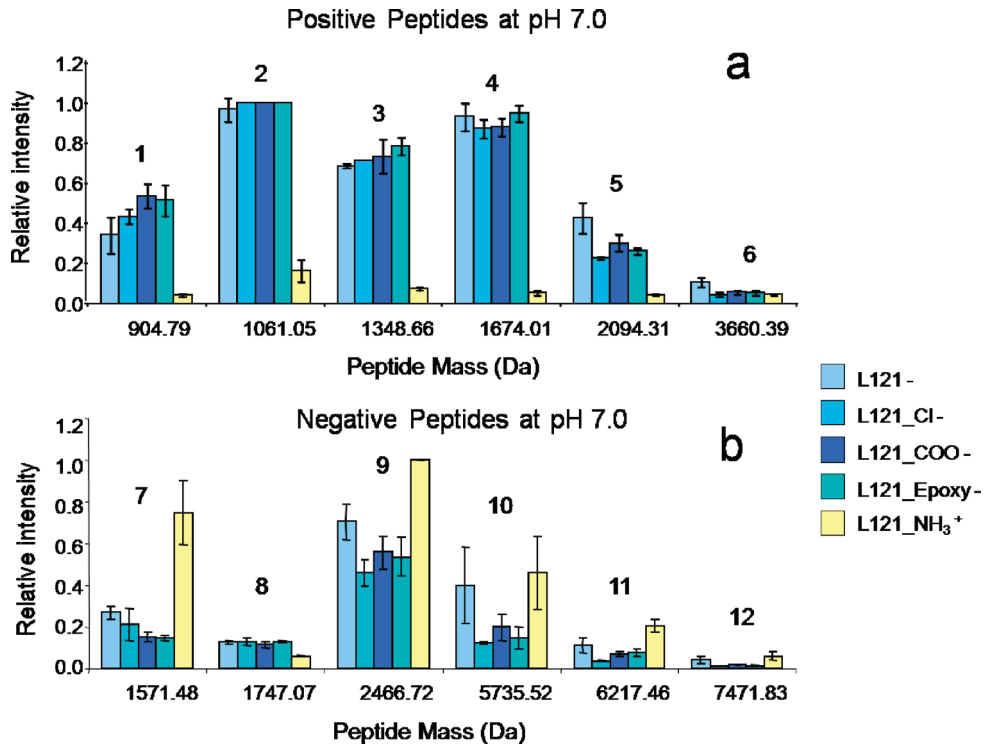

Figure 11. Charge-specific recovery for the chips with different surface functions. Bar graph of the MS intensity of detection of selectively captured peptides on the functionalized chips. According to their iso-electric point, the peptides are positively or negatively charged at pH 7.0. (a) Positive peptides ((1) des-Arg1-Bradykinin, (2) Bradykinin, (3) substance P-amide, (4) Neurotensin, (5) ACTH(1−17), (6) ACTH(7−38)) are specifically enriched on the negatively charged surfaces. (b) Negative peptides ((7) Glu1-fibrinopeptide B, (8) α-endorphin, (9) ACTH(18−39), (10) insulin, (11) EGF, (12) insulin-like GFII) are specifically enriched on the positively charged surfaces.

Different MPS thin film periodic nanostructures, formed using high molecular weight triblock copolymers such as Pluronic F127 with similar pore size distributions, were obtained by tuning the polymer concentration in the precursor solution. The 3D cubic and honeycomb hexagonal nanostructures, possessing more desirable nanopore interconnectivity and more accessible nanopore morphology, exhibited superior performance in selectively enriching LMW peptides than the 2D hexagonal structure, even though they share similar pore size distributions and the same molecular cutoff for serum fractionation. Precisely controlled variations in pore size were achieved through the use of copolymers with differing hydrophobic block lengths. The effect of pore size on the peptides and LMW proteins' recovery efficacy was investigated using MPS thin films prepared from four Pluronic surfactants (F127, P123, L64, L121, and L121 plus swelling agent) with different volume ratios of the hydrophilic and hydrophobic components to form pore sizes of 3, 4, 6, and 7 nm, respectively. Although all of these MPS chips possess a 3D nanostructure, the wide range of pore sizes led to the recovery of a different repertoire of peptides and proteins from the same serum sample *via* size and shape exclusion. We also streamlined the conjugation of organo-silane on MPS chips by introducing oxygen plasma ashing to pretreat the chip surface. Besides the depletion of HMW proteins, the results demonstrated that the structural design and the chemical functionalization of the MPS further increased the specificity of peptide enrichment. The individual or integral use of different MPS thin films with carefully tailored characteristics provides a novel platform for the rapid and efficient analysis of the LMWP in human serum and may be implemented for the discovery of novel proteomic biomarkers.

METHODS

Fabrication of Mesoporous Silica Thin Films. As listed in Table 1 in the Supporting Information, the molar ratios of starting materials are slightly different for various surfactants. A typical preparation of the coating sol was carried out as follows: the required amount of TEOS was dissolved in the mixture of ethanol, distilled water, and 2 M HCl and stirred for 1 h at 75 °C to form a clear silicate sol. Separately, a portion of surfactant was dissolved in ethanol by stirring at room temperature. In the case of applying the swelling agent, the amount of PPG solution was put into the surfactant solution with vigorous stirring at room temperature. The coating solution was prepared by mixing the silicate sol into the triblock copolymer solution followed by stirring of the resulting sol for 2 h at room temperature. The pH of the mixture solution remained around 1.5. The coating sol was deposited on a Si(100) wafter by spin coating at the spin rate of 2500 rpm for 20 s. To increase the degree of polymerization of the silica framework in the films and to further improve their thermal sta-

bility, the as-deposited films were heated at 80 °C for 12 h. The films were calcinated at 425 °C to remove the organic surfactant. The temperature was raised at a heating rate of 1 °C/min, and the furnace was heated at 425 °C for 5 h. The films produced were transparent and crackless.

Chemical Modification. Oxygen plasma ashing was performed in a Plasma Asher (March Plasma System) to pretreat the MPS chip surface. The treatment was carried out with an O_2 flow rate at 80 sccm and a power of 300 W for 10 min. Then the chips were silanated in a 3% organosilane in a methanol/DI water (19:1) solution for 72 h at room temperature in a N_2 glovebox. After this, they were rinsed sequentially with methanol and DI water. Finally, the chips were cured at 110 °C for 15 min in a fan-operated oven.

Characterization Techniques. We utilized several characterization techniques to study the spin-coated mesoporous silica thin films. By using a variable angle spectroscopic ellipsometer (J. A. Woollam Co. M-2000DI) and modeling with WVASE32 software, the thickness of thin films and their porosities were measured in Cauchy and effective medium approximation (EMA) models, respectively. Ellipsometric optical quantities, the phase (Δ) and amplitude (Ψ) were carried by requiring spectra for 65, 70, and 75° incidence angles using wavelengths from 300 to 1800 nm. In the Cauchy model, the top layer's thickness, reflective index, and model fit parameters A_n, B_n, and C_n were determined by fitting experimental data with the model and minimizing the mean square error (usually less than 10). Using the EMA model, the films' porosities were calculated by assuming a certain volume of void in the pure silica and setting the top layer's thickness obtained by the Cauchy model as the constant. X-ray diffraction (XRD) patterns were obtained on Philips X'Pert-MPD system with Cu Kα ray (45 kV, 40 mA); $\theta-2\theta$ scanning was recorded from all spin-coated films at 1 s/0.001° step over the angle range from 0.2 to 6°. Scanning transmission electron microscopy (STEM; FEI Technai; FEI Co.) was used in acquiring micrographs of the plane view of mesoporous silica thin films at high tension of 200 kV. Contact angles of film surface were measured by goniometer with captive bubble contact angle measurement. N_2 adsorption/desorption analysis was applied in measuring surface area and pore size distribution. Quantachrome was used to record the N_2 adsorption/desorption isotherm at 77 K on the full range of relative P/P_0 pressures. Brunauer−Emmett−Teller (BET) surface areas were determined over a relative pressure range of 0.05 to 0.3. Nanopore size distributions were calculated from the desorption branch of the isotherms using Barrett−Joyner−Halenda (BJH) method. XPS spectra were recorded using a X-ray photoelectron spectrometer (Kratos Axis Ultra), utilizing a monochromated Al Kα X-ray source ($h\nu = 1486.5$ eV), hydrid optics (employing a magnetic and electrostatic lens simultaneously), and a multichannel plate and delay line detector coupled to a hemispherical analyzer. The photoelectron's take off angle was 90°. All spectra were recorded using an aperture slot of 300 × 700 μm, and high-resolution spectra were collected with a pass energy of 20 eV. The pressure in the analysis chamber was typically 2×10^{-9} Torr during data acquisition. Kratos XPS analysis software was used to determine the stoichiometry of samples from corrected peak areas and employing Kratos sensitivity factors for each element of interest.

Serum Fractionation. For each experiment, a 10 μL sample of serum was pipetted onto the porous surface of the wafer square. The samples were incubated for 30 min at 25 °C (room temperature) in a wet chamber (100% humidity) to prevent sample evaporation. The samples were washed five times with 15 μL of sterile, deionized water. Peptides and proteins were eluted from the pores using a 1:1 (v/v) mixture of acetonitrile and 0.1% trifluoroacetic acid (TFA) (Sigma).

Mass Spectrometry. A matrix solution of 5 mg/mL α-cyano-4-hydroxycinnamic acid (CHCA, Sigma) in a 1:1 mixture of acetonitrile and 0.1% TFA (v/v) or a saturated solution of *trans*-3,5-dimethoxy-4-hydroxycinnamic acid (SA, Sigma) in 2:1 mixture of acetonitrile and water (v/v) containing 0.1% TFA was used for LMW and HMW analysis, respectively. Each of the samples was mixed with the appropriate matrix in a ratio of 1:3 and spotted in duplicate onto the MALDI plate.

Mass spectra were acquired on a Voyager-DE-STR MALDI-TOF (Applied Biosystems, Framingham, MA) mass spectrometer in linear positive-ion mode, using a 337 nm nitrogen laser. Samples were evaluated at two *m/z* ranges. For the peptides and LMW proteins with the *m/z* of 800−10 000 Da, we used α-CHCA as the matrix. Settings were optimized at an acceleration voltage 20 kV, grid voltage of 19 kV, guide wire voltage of 1 kV, delay time of 180 ns, and low-mass gate of 800. Three hundred laser shots crossed spot were averaged for each mass spectrum. For HMW proteins, parallel analysis using SA (sinapinic acid) as the matrix and detection range of 3000−100 000 Da was performed. The instrument was optimized at acceleration voltage 25 kV, grid voltage of 23.25 kV, guide wire voltage of 6.25 kV, delay time of 500 ns, and low mass gate of 3000.

The spectra were calibrated externally using the ProteoMass standards of peptides and proteins (Sigma) in each mass range. The raw spectra were processed with the Voyager Data Explorer software version 4.0 (Applied Biosystems).

Statistical Analysis. The raw spectra were processed with the Voyager Data Explorer software version 4.0 (Applied Biosystems), and the data were exported to SpecAlign software for pretreatment.[57,58] All spectra were aligned using the PAFFT correlation method, and intensities were normalized to total ion current (TIC). The peak detection was performed with a height ratio of 2 with 0.3% of the mass window, the baseline was corrected, and the negative values were removed prior to analysis.

Hierarchical clustering was performed using Cluster software and visualized with MapleTree software.[59] MALDI MS data (*m/z* peak intensities) were log-transformed, normalized, and median centered. Pearson correlation was used to calculate the distance between the samples, and complete linkage clustering was performed. An independent student *t* test was used for comparison between groups ($n = 2$ groups) for each detected MS peak prior to supervised hierarchical clustering analysis. A *P* value of 0.02 or lower was considered significant to select differentially harvested peptides and proteins among the different mesoporous proteomic chips (large pores *vs* small pores).

Acknowledgment. The authors thank Prof. Rowen Chang and the Research Center of Protein Chemistry Core Laboratory at the University of Texas Health Science Center at Houston for carrying out mass spectroscopy. We thank Dr. Hugo Celio, the facility manager in the Center of Nanomaterial at the University of Texas at Austin, for providing the assistance in XPS measurement, and the NSF (Grant No. 0618242) for funding the X-ray photoelectron spectrometer used in this work. We also thank Dr. Daniel H. Fine and Jeffery Schmulen for their help on this project. These studies were supported by the following grants: State of Texas's Emerging Technology Fund, NIH (R21/R33CA122864), NASA (NNJ06HE06A), NIH (R01CA128797), DoD CDMRP Breast Cancer Research Program Innovator Award (W81XWH-08-BCRP-INNOV). The authors would like to recognize the contributions and support from the Alliance for NanoHealth (ANH).

Supporting Information Available: Molar ratio of starting materials used to fabricate the MPS thin films and their final physical properties, physicochemical properties (molecular weight and iso-electric point) of the selected peptide and protein standards, the protocol of on-chip serum fractionation, MS profiles of reproducibility of on-chip fractionation, XRD spectra and STEM images of MPS thin films prepared using different polymer templates, contact angle goniometry for MPS thin films, mass spectra of the proteins and peptides collected from samples fractionated using chips prepared with different polymer templates, the protocol of pretreatment on MPS surface with oxygen plasma, XPS spectra of mesoporous silica chips with negative charged modification, MS profiles of selectively captured or excluded proteins on the chemically modified chips. This material is available free of charge *via* the Internet at http://pubs.acs.org.

REFERENCES AND NOTES

1. Lu, Y.; Ganguli, R.; Drewien, C. A.; Anderson, M. T.; Brinker, C. J.; Gong, W.; Guo, Y.; Soyez, H.; Dunn, B.; Huang, M. H.;

Zink, J. I. Continuous Formation of Supported Cubic and Hexagonal Mesoporous Films by Sol−Gel Dip-Coating. *Nature* **1997**, *389*, 364–368.
2. Zhao, D.; Yang, P.; Melosh, N.; Feng, J.; Chmelka, B. F.; Stucky, G. D. Continuous Mesoporous Silica Films with Highly Ordered Large Pore Structures. *Adv. Mater.* **1998**, *10*, 1380–1385.
3. Wan, Y.; Shi, Y.; Zhao, D. Designed Synthesis of Mesoporous Solids via Nonionic-Surfactant-Templating Approach. *Chem. Commun.* **2007**, *9*, 897–926.
4. Sanchez, C; Boissiere, C.; Grosso, D.; Laberty, C.; Nicole, L. Design, Synthesis, and Properties of Inorganic and Hybrid Thin Films Having Periodically Organized Nanoporosity. *Chem. Mater.* **2008**, *20*, 682–737.
5. Maschmeyer, T.; Rey, F.; Sankar, G.; Thomas, J. M. Heterogeneous Catalysts Obtained by Grafting Metallocene Complexes onto Mesoporous Silica. *Nature* **1995**, *378*, 159–162.
6. Liu, J.; Yang, Q.; Kapoor, M. P.; Setoyama, N.; Inagaki, S.; Yang, J.; Zhang, L. Structural Relation Properties of Hydrothermally Stable Functionalized Mesoporous Organosilicas and Catalysis. *J. Phys. Chem. B* **2005**, *109*, 12250–12256.
7. Wan, Y.; Wang, H.; Zhao, Q.; Klingstedt, M.; Terasaki, O.; Zhao, D. Ordered Mesoporous Pd/Silica-Carbon as a Highly Active Heterogeneous Catalyst for Coupling Reaction of Chlorobenzene in Aqueous Media. *J. Am. Chem. Soc.* **2009**, *131*, 4541–4550.
8. Thomas, J. M.; Hernandez-Garrido, J. C.; Raja, R.; Bell, R. G. Nanoporous Oxidic Solids: The Confluence of Heterogeneous and Homogeneous Catalysis. *Phys. Chem. Chem. Phys.* **2009**, *11*, 2799–2825.
9. Kresge, C. T.; Leonowicz, M. E.; Roth, W. J.; Vartuli, J. C.; Beck, J. S. Ordered Mesoporous Molecular Sieves Synthesized by a Liquid-Crystal Template Mechanism. *Nature* **1992**, *359*, 710–712.
10. Tanev, P. T.; Pinnavaia, T. J. Mesoporous Silica Molecular Sieves Prepared by Ionic and Neutral Surfactant Templating: A Comparison of Physical Properties. *Chem. Mater.* **1996**, *8*, 2068–2079.
11. Bagshaw, S. A.; Prouzet, E.; Pinnavaia, T. J. Templating of Mesoporous Molecular Sieves by Nonionic Polyethylene Oxide Surfactants. *Science* **1995**, *269*, 1242–1244.
12. Yiu, H. H. P.; Wright, P. A. Enzymes Supported on Ordered Mesoporous Solids: a Special Case of an Inorganic−Organic Hybrid. *J. Mater. Chem.* **2005**, *15*, 3690–3700.
13. Rossinyol, E.; Arbiol, J.; Peir, F.; Cornet, A.; Morante, J. R.; Tian, B.; Bo, T.; Zhao, D. Nanostructured Metal Oxides Synthesized by Hard Template Method for Gas Sensing Applications. *Sens. Actuators, B* **2005**, *109*, 57–63.
14. Scott, B. J.; Wirnsberger, G.; Stucky, G. D. Mesoporous and Mesostructured Materials for Optical Applications. *Chem. Mater.* **2001**, *13*, 3140–3150.
15. Yamada, T.; Zhou, H.; Uchida, H.; Honma, I.; Katsube, T. Experimental and Theoretical NOx Physisorption Analyses of Mesoporous Film (SBA-15 and SBA-16) Constructed Surface Photo Voltage (SPV) Sensor. *J. Phys. Chem. B* **2004**, *108*, 13341–13346.
16. Yamada, T.; Zhou, H.-S.; Uchida, H.; Tomita, M.; Ueno, Y.; Ichino, T.; Honma, I.; Asai, K.; Katsube, T. Surface Photovoltage NO Gas Sensor with Properties Dependent on the Structure of the Self-Ordered Mesoporous Silicate Film. *Adv. Mater.* **2002**, *14*, 812–815.
17. Sel, O.; Sallard, S.; Brezesinski, T.; Rathousky, J.; Dunphy, D. R.; Collord, A.; Smarsly, B. M. Periodically Ordered Meso- and Macroporous SiO_2 Thin Films and Their Induced Electrochemical Activity as a Function of Pore Hierarchy. *Adv. Funct. Mater.* **2007**, *17*, 3241–3250.
18. Mal, N. K.; Fujiwara, M.; Tanaka, Y. Photocontrolled Reversible Release of Guest Molecules from Coumarin-Modified Mesoporous Silica. *Nature* **2003**, *421*, 350–353.
19. Munoz, B.; Ramila, A.; Perez-Pariente, J.; Diaz, I.; Vallet-Regi, M. MCM-41 Organic Modification as Drug Delivery Rate Regulator. *Chem. Mater.* **2002**, *15*, 500–503.
20. Vallet-Regi, M.; Ramila, A.; del Real, R. P.; Perez-Pariente, J. A New Property of MCM-41: Drug Delivery System. *Chem. Mater.* **2000**, *13*, 308–311.
21. Lai, C.-Y.; Trewyn, B. G.; Jeftinija, D. M.; Jeftinija, K.; Xu, S.; Jeftinija, S.; Lin, V. S. Y. A Mesoporous Silica Nanosphere-Based Carrier System with Chemically Removable CdS Nanoparticle Caps for Stimuli-Responsive Controlled Release of Neurotransmitters and Drug Molecules. *J. Am. Chem. Soc.* **2003**, *125*, 4451–4459.
22. Slowing, I. I.; Trewyn, B. G.; Giri, S.; Lin, V. S.-Y. Mesoporous Silica Nanoparticles for Drug Delivery and Biosensing Applications. *Adv. Funct. Mater.* **2007**, *17*, 1225–1236.
23. Zhao, J.; Gao, F.; Fu, Y.; Jin, W.; Yang, P.; Zhao, D. Biomolecule Separation Using Large Pore Mesoporous SBA-15 as a Substrate in High Performance Liquid Chromatography. *Chem. Commun.* **2002**, *7*, 752–753.
24. Kuo, C.-W.; Shiu, J.-Y.; Wei, K. H.; Chen, P. Monolithic Integration of Well-Ordered Nanoporous Structures in the Microfluidic Channels for Bioseparation. *J. Chromatogr. A* **2007**, *1162*, 175–179.
25. Deere, J.; Magner, E.; Wall, J. G.; Hodnett, B. K. Mechanistic and Structural Features of Protein Adsorption onto Mesoporous Silicates. *J. Phys. Chem. B* **2002**, *106*, 7340–7347.
26. Brinker, J.; Lu, Y,; Sellinger, A.; Fan, H. Evaporation-Induced Self-Assembly: Nanostructures Made Easy. *Adv. Mater.* **1999**, *11*, 579–585.
27. Cheng, M. M.-C.; Cuda, G.; Bunimovich, Y. L.; Gaspari, M.; Heath, J. R.; Hill, H. D.; Mirkin, C. A.; Nijdam, A. J.; Terracciano, R.; Thundat, T.; Ferrari, M. Nanotechnologies for Biomolecular Detection and Medical Diagnostics. *Curr. Opin. Chem. Biol.* **2006**, *10*, 11–19.
28. Terracciano, R.; Gaspari, M.; Testa, F.; Pasqua, L.; Tagliaferri, P.; Cheng, M. M.; Nijdam, A. J.; Petricoin, E. F.; Liotta, L. A.; Cuda, G.; Ferrari, M.; Venuta, S. Selective Binding and Enrichment for Low-Molecular Weight Biomarker Molecules in Human Plasma after Exposure to Nanoporous Silica Particles. *Proteomics* **2006**, *6*, 3243–3250.
29. Geho, D.; Ming-Cheng Cheng, M.; Killian, K.; Lowenthal, M.; Ross, S.; Frogale, K.; Nijdam, J.; Lahar, N.; Johann, D.; Herrmann, P.; Whiteley, G.; Ferrari, M.; Petricoin, E.; Liotta, L. Fractionation of Serum Components Using Nanoporous Substrates. *Bioconjugate Chem.* **2006**, *17*, 654–661.
30. Gaspari, M.; Ming-Cheng Cheng, M.; Terracciano, R.; Liu, X.; Nijdam, A. J.; Vaccari, L.; di Fabrizio, E.; Petricoin, E. F.; Liotta, L. A.; Cuda, G.; Venuta, S.; Ferrari, M. Nanoporous Surfaces as Harvesting Agents for Mass Spectrometric Analysis of Peptides in Human Plasma. *J. Proteome Res.* **2006**, *5*, 1261–1266.
31. Wulfkuhle, J. D.; Liotta, L. A.; Petricoin, E. F. Proteomic Applications for the Early Detection of Cancer. *Nat. Rev. Cancer* **2003**, *3*, 267–275.
32. Ebert, M. P. A.; Meuer, J.; Wiemer, J. C.; Schulz, H.-U.; Reymond, M. A.; Traugott, U.; Malfertheiner, P.; Rocken, C. Identification of Gastric Cancer Patients by Serum Protein Profiling. *J. Proteome Res.* **2004**, *3*, 1261–1266.
33. Etzioni, R.; Urban, N.; Ramsey, S.; McIntosh, M.; Schwartz, S.; Reid, B.; Radich, J.; Anderson, G.; Hartwell, L. The Case for Early Detection. *Nat. Rev. Cancer* **2003**, *3*, 243–252.
34. Hanash, S. M.; Pitteri, S. J.; Faca, V. M. Mining the Plasma Proteome for Cancer Biomarkers. *Nature* **2008**, *452*, 571–579.
35. Kulasingam, V.; Diamandis, E. P. Strategies for Discovering Novel Cancer Biomarkers through Utilization of Emerging Technologies. *Nat. Clin. Prac. Oncol.* **2008**, *5*, 588–599.
36. Liotta, L. A.; Ferrari, M.; Petricoin, E. Clinical Proteomics: Written in Blood. *Nature* **2003**, *425*, 905.
37. Petricoin, E. F.; Belluco, C.; Araujo, R. P.; Liotta, L. A. The Blood Peptidome: A Higher Dimension of Information Content for Cancer Biomarker Discovery. *Nat. Rev. Cancer* **2006**, *6*, 961–967.
38. Villanueva, J. Differential Exoprotease Activities Confer Tumor-Specific Serum Peptidome Patterns. *J. Clin. Invest.* **2006**, *116*, 271–284.

39. Anderson, N. L.; Anderson, N. G. The Human Plasma Proteome: History, Character, and Diagnostic Prospects. *Mol. Cell Proteomics* **2002**, R200007-MCP200.
40. Görg, A.; Weiss, W.; Dunn, M. J. Current Two-Dimensional Electrophoresis Technology for Proteomics. *Proteomics* **2004**, *4*, 3665–3685.
41. Liu, H.; Sadygov, R. G.; Yates, J. R. A Model for Random Sampling and Estimation of Relative Protein Abundance in Shotgun Proteomics. *Anal. Chem.* **2004**, *76*, 4193–4201.
42. Rabilloud, T. Two-Dimensional Gel Electrophoresis in Proteomics: Old, Old Fashioned, But It Still Climbs up the Mountains. *Proteomics* **2002**, *2*, 3–10.
43. Lim, M. H.; Blanford, C. F.; Stein, A. Synthesis and Characterization of a Reactive Vinyl-Functionalized MCM-41: Probing the Internal Pore Structure by a Bromination Reaction. *J. Am. Chem. Soc.* **1997**, *119*, 4090–4091.
44. Mercier, L.; Pinnavaia, T. J. Direct Synthesis of Hybrid Organic-Inorganic Nanoporous Silica by a Neutral Amine Assembly Route: Structure−Function Control by Stoichiometric Incorporation of Organosiloxane Molecules. *Chem. Mater.* **1999**, *12*, 188–196.
45. Lu, Y.; Fan, H.; Doke, N.; Loy, D. A.; Assink, R. A.; LaVan, D. A.; Brinker, C. J. Evaporation-Induced Self-Assembly of Hybrid Bridged Silsesquioxane Film and Particulate Mesophases with Integral Organic Functionality. *J. Am. Chem. Soc.* **2000**, *122*, 5258–5261.
46. Asefa, T.; MacLachlan, M. J.; Coombs, N.; Ozin, G. A. Periodic Mesoporous Organosilicas with Organic Groups Inside the Channel Walls. *Nature* **1999**, *402*, 867–871.
47. Inagaki, S.; Guan, S.; Ohsuna, T.; Terasaki, O. An Ordered Mesoporous Organosilica Hybrid Material with a Crystal-like Wall Structure. *Nature* **2002**, *416*, 304–307.
48. Brunel, D.; Cauvel, A.; Fajula, F.; DiRenzo, F.; Laurent, B.; Serge, K. MCM-41 Type Silicas as Supports for Immobilized Catalysts. In *Studies in Surface Science and Catalysis*; Elsevier: Amsterdam, 1995; Vol. 97, pp 173−180.
49. Brunel, D. Functionalized Micelle-Templated Silicas (MTS) and Their Use as Catalysts for Fine Chemicals. *Microporous Mesoporous Mater.* **1999**, *27*, 329–344.
50. Brunel, D.; Blanc, A. C.; Galarneau, A.; Fajula, F. New Trends in the Design of Supported Catalysts on Mesoporous Silicas and Their Applications in Fine Chemicals. *Catal. Today* **2002**, *73*, 139–152.
51. Diamandis, E. P. Mass Spectrometry as a Diagnostic and a Cancer Biomarker Discovery Tool: Opportunities and Potential Limitations. *Mol. Cell Proteomics* **2004**, *3*, 367–378.
52. Petricoin, E. F.; Zoon, K. C.; Kohn, E. C.; Barrett, J. C.; Liotta, L. A. Clinical Proteomics: Translating Benchside Promise into Bedside Reality. *Nat. Rev. Drug Discovery* **2002**, *1*, 683–695.
53. Villanueva, J; Philip, J.; Chaparro, C. A.; Li, Y.; Toledo-Crow, R.; DeNoyer, L.; Fleisher, M.; Robbins, R. J.; Tempst, P. Correcting Common Errors in Identifying Cancer-Specific Serum Peptide Signatures. *J. Proteome Res.* **2005**, *4*, 1060–1072.
54. Findeisen, P.; Sismanidis, D.; Riedl, M.; Costina, V.; Neumaier, M. Preanalytical Impact of Sample Handling on Proteome Profiling Experiments with Matrix-Assisted Laser Desorption/Ionization Time-of-Flight Mass Spectrometry. *Clin. Chem.* **2005**, *51*, 2409–2411.
55. Seam, N.; Gonzales, D. A.; Kern, S. J.; Hortin, G. L.; Hoehn, G. T.; Suffredini, A. F. Quality Control of Serum Albumin Depletion for Proteomic Analysis. *Clin. Chem.* **2007**, *53*, 1915–1920.
56. Barrett, E. P.; Joyner, L. G.; Halenda, P. P. The Determination of Pore Volume and Area Distributions in Porous Substances. I. Computations from Nitrogen Isotherms. *J. Am. Chem. Soc.* **1951**, *73*, 373–380.
57. Wong, J. W. H.; Cagney, G.; Cartwright, H. M. SpecAlign--Processing and Alignment of Mass Spectra Datasets. *Bioinformatics* **2005**, *21*, 2088–2090.
58. Wong, J. W. H.; Durante, C.; Cartwright, H. M. Application of Fast Fourier Transform Cross-Correlation for the Alignment of Large Chromatographic and Spectral Datasets. *Anal. Chem.* **2005**, *77*, 5655–5661.
59. Eisen, M. B.; Spellman, P. T.; Brown, P. O.; Botstein, D. Cluster Analysis and Display of Genome-Wide Expression Patterns. *Proc. Natl. Acad. Sci. U.S.A.* **1998**, *95*, 14863–14868.